Modeling and Optimization of Nd:YAG Laser-TIG Hybrid Welding of Stainless Steel

Moradi, M., Ghoreishi, M. & Khorram, A.

Original citation & hyperlink:
Moradi, M, Ghoreishi, M & Torkamany, MJ 2014, 'Modeling and Optimization of Nd:YAG Laser-TIG Hybrid Welding of Stainless Steel', Lasers in Engineering, vol. 27, no. 3-4, pp. 211-230.

http://www.oldcitypublishing.com/journals/lie-home/lie-issue-contents/lie-volume-27-number-3-4-2014/
ISSN 0898-1507
ESSN 1029-029X

Publisher: Old City Publishing

Modeling and optimization of Nd:YAG laser-TIG hybrid welding of stainless steel

M. Moradi[1], M. Ghoreishi[1], M. J. Torkamany[2]

[1]Faculty of Mechanical Engineering, K.N. Toosi University of Technology, P. O. Box 1999143344, Tehran, Iran

[2] Iranian National Centre for Laser Science and Technology, P.O. Box 14665-576, Tehran, Iran

ABSTRACT

In the present study the Nd:YAG laser-tungsten inert gas (TIG) hybrid butt joint welding (LATIG) parameters of stainless steel 1.4418 have been investigated by coupling a pulsed Nd:YAG laser with a CW TIG source. The experiments were performed based on the Response Surface Methodology (RSM) as a statistical design of experiments approach to investigate the effect of parameters on the response variations, and achieve the mathematical equations to predict the new results. Welding speed (1 to 5mm/s), TIG Current (90to 130 A) and distance of heat sources (1 to 5 mm) were assumed as the input process variables while the weld surface width (W), weld seam area (A), and weld penetration (P) were considered as the process responses. Analyzed by statistical techniques, the results indicated that the welding speed is the most important parameter among all parameters with a reverse effect on process outputs. Besides, TIG current has a direct influence on all investigated responses. The paper invokes the desirability approach optimization technique to achieve the best geometrical dimensions of weld profiles and validating the theoretical results using the experimental tests. Once the optimum settings are considered, a tensile test was also conducted.

Keywords**: Laser-TIG hybrid welding, Design of Experiments, Response Surface Methodology, weld bead profile**

1. INTRODUCTION

The history of laser-arc hybrid welding goes back to more than 30 years ago. The hybrid laser-arc welding process overcomes deficiencies encountered with each individual process and has its own particular advantages, such as the deeper weld penetration, fewer deformation, high welding speed, the ability to bridge relatively large gaps, capability of welding highly reflective materials and improvement at arc stability [1]. Because of these advantages, laser-arc hybrid welding technologies have become more popular in recent years and have strong industrial application, including aerospace, automotive, off-road vehicle, shipbuilding, oil and pressure vessel industries, etc[2]. In the laser-TIG (LATIG) technique, a TIG torch is placed on axis with a laser beam, and both are aligned with the welding direction. The electric arc dilutes the electron density of laser plasma, weakens the ability of laser plasma to absorb and reflect the laser energy, so it improves the heat efficiency of laser beams[3].

Design of experiments (DOE) and statistical techniques are widely used to analyze and optimize process parameters[4]. To obtain the high-quality joint, choosing the process input parameters has a vital role. In last two decades, the application of one of the DOE approaches, the Response Surface Methodology (RSM), for prediction the certain features of the welds output parameters and also for optimization different parameters process, was of high interest among researchers [5-7]. Some advantages of RSM could be proper reduction in the number of experiment, such as consideration of all parameter's variation and interaction effects and, the development of mathematical functions to achieve a logical relationship between input and output parameters. Curvatures on the developed response surfaces (3D plots) created suitable use of RSM. In addition, it shows that the process parameter ranges have been selected correctly and the optimum setting would exist in the considered parameters space.

Liming et al. [3] made a comparison between hybrid laser-TIG welding, laser welding, and TIG welding of AZ31B alloy in the weldability and microstructure characteristic. Liming et al. showed that penetration of hybrid welding is two times that of TIG and four times that of laser beam welding. Mechanical and metallurgical properties of hybrid laser-TIG welding on 304 steel was investigated by Yan et al.[8]. they reported that the maximum and minimum tensile strengths occur in the alone laser welding and TIG welding respectively. Some experiments reported that hybrid welding cannot improve the penetration [9]. Zhiyong Li et al. [10], calculated electronic temperature in Nd:YAG laser–MIG hybrid welding using the Boltzmann plot method and the electronic density by using the Stark broadening method. Casalino [11] investigated MIG-CO_2 laser hybrid welding of AlMg alloy using the DOE method. In Casalino researches laser power, focal position, heat sources distance and torch angle were selected as input parameters, in which the weld penetration was the only output of the design. CO_2 laser butt-welding parameters of Ti6Al4V alloy was analyzed using response surface methodology as one of the DOE methods by khorram and ghoreishi [12]. Javid et al. [13] was developed a three-dimensional finite element model to simulate the laser beam welding and calculate the transient temperature profile and dimensions of the fusion zone and heat affected zone (HAZ) during the laser welding process. The Nd:YAG laser was also used in hybrid welding for welding of aluminum and steel on the benefit of its short wavelength, 1064 nm [14]. Turbulent flow in the weld pool has also been linked with porosity formation and studied by Kim et al [15]. SujitGhosal et al [16] invokes artificial neural network to predict and optimizes weld penetration in CO2 laser-Mig hybrid welding of aluminum alloy 5005. A general review and complete bibliography of laser hybrid processes is prepared by Bagger and Olsen recently [17].

The purpose of the present study is investigating the effect of Laser-TIG hybrid welding process parameters, including welding speed (S), TIG Current (I) and distance of heat sources (DLA) on the melt pool shape of stainless steel 1.4418 samples, through the Response Surface Methodology (RSM). Weld surface width (W), weld seam area (A), and penetration (P), are the three process responses considered by the statistical analysis. Figure 1 shows the cross section of a typical welding sample and positions used to recognize the considered responses in this study. Optimization of the Laser-TIG hybrid welding parameters were carried out in order to access the minimum geometrical dimensions of weld-bead profile according to achieved mathematical models. In order to validate the results of optimization, welding experiments were carried out using the optimum parameters.

2-EXPERIMENTAL DESIGN AND METHODOLOGY

2.1 Response Surface Methodology (RSM)

Process of modeling is generally influenced by the method which has been chosen for conducting and designing experiments. One of these methods is RSM, which is a set of mathematical and statistical techniques that is useful for modelling and predicting the desired response[18, 19]. Furthermore, RSM specifies the relationships between one or more measured responses and the essential controllable input factors[20]. When all independent variables are measurable and experiments can be repeated with negligible errors, the RSM could be defined using equation (1):

$$Y = f(x_1, x_2, x_3, \ldots, x_k) \qquad (1)$$

where k is the number of independent variables.

Finding a function to relate the independent variables and the responses is essential. Generally, second-order (quadratic) polynomial is used in RSM to precise the model and responses as follows:

$$y = \beta_0 + \sum_{i=1}^{k} \beta_i x_i + \sum_{i=1}^{k} \beta_{ii} x_i^2 + \sum_{i} \sum_{j} \beta_{ij} x_i x_j + \varepsilon \qquad (2)$$

Where, β_0 is the constant value or intercept, β_i linear coefficient, β_{ii} quadratic coefficient, β_{ij} interaction coefficient and ε is the random error of the developed regression[20].

Linear and second order polynomials were found best to fit to the experimental data, using the sequential *F-test*, *T-test*. *Lack-of-fit test* and other adequacy measures were also employed to validate the accuracy of developed regression equations. Curvatures on the developed response surfaces (3D plots) show that the parameter ranges of process have been selected correctly and the optimum setting would exist in the considered parameters space.

2.2 Desirability approach

Many response surface problems deal with the analysis of several responses. Simultaneous consideration of multiple responses, involve first building an appropriate response surface model for each response and then trying to find a set of optimized operating condition; which optimizes all responses or at least keeps them in desired ranges. Due to its simplicity, availability in the software and flexibility provision in weighting and giving importance for the individual response, the desirability method is recommended. Desirability method is a simultaneous optimization technique which was popularized by Drringer and Suichin 1980[21]. Solving multiple response optimization problems employing this technique starts with using a technique for combining multiple responses into a dimensionless measure of performance called the overall desirability function. The general approach is to convert each response Y_i into a dimensionless utility bounded by $0<d_i<1$, where a higher d_i value indicates that response value Y_i is more desirable, and if the response is outside an acceptable region, $d_i=0$ then the design variables are chosen to maximize the overall desirability, eq. 3 [4]:

$$D= (d_1.d_2\ldots.d_m)^{1/m} \qquad (3)$$

Where, m is the number of responses.

In the current work, the individual desirability of each response, d_i,is calculated using Eqs. (4)–(6). The shape of the desirability function depends on the weight field 'r'. To emphasize on the target value, Weights are invoked. When the weight value equals 1, the desirability function will be in linear mode. Choosing r>1 places more emphasis on being close to the target value, and choosing 0<r<1 makes this less important [12]. If the target T for the response y is a maximum value, the desirability will be defined by, eq. 4:

$$d = \begin{cases} 0 & y < L \\ \left(\frac{y-L}{T-L}\right)^r & L \leq y \leq T \\ 1 & y > T \end{cases} \qquad (4)$$

For a minimum goal function, the desirability is defined using eq. 5:

$$d = \begin{cases} 1 & y < L \\ \left(\frac{T-y}{T-L}\right)^r & L \leq y \leq T \\ 0 & y > T \end{cases} \qquad (5)$$

If the target is located between the lower (L) and upper (U) limits, the desirability will be defined by, eq. 6:

$$d = \begin{cases} 0 & y < L \\ \left(\frac{y-L}{T-L}\right)^r & L \leq y \leq T \\ \left(\frac{U-y}{U-T}\right)^r & T \leq y \leq U \\ 0 & y > U \end{cases} \qquad (6)$$

3- EXPERIMENTAL PROSEDURES:

In this study, stainless steel 1.4418 sheets (254mm × 38mm) with thickness of 4 mm were used as the material work piece which is used in the compressor shaft of the gas turbine. The welding process in the shaft is EBW and for replacing the EBW process by laser hybrid arc welding (LHAW) this study is performed to obtain the optimum parameters of the LHAW. The chemical composition of the material, which is the average of three X-ray fluorescence (XRF) measurements, is presented in table 1.

In the experiments a pulsed Nd:YAG laser model IQL-10 with a maximum mean laser power of 400 W was used as a laser source combined with a direct current electrode negative TIG (DCEN-TIG) arc with a maximum current of 250 amperes. Square shape pulses are the standard output of this laser. The available range for the laser parameters was 1–1000 Hz for pulse frequency, 0.2–20 ms for pulse duration, and 0–40 J for pulse energy. Since the average laser power could not be more than 400W, it is evident that no arbitrary combination of pulse energy and pulse frequency could be used. The focusing length of laser beam is 75 mm with 250 μm minimum spot size. A 5000W-Lp Ophir power meter and LA300W-LP joule meter were used to measure average power and pulse energy. Details of the experimental setup can be found in [22].

Figure 2 shows a schematic drawing of the laser-TIG hybrid welding process. As shown in this figure, the arc is leading, no filler metal is used and the laser is vertical to the base metal and the TIG torch is placed with a 35 degree angle to the horizontal surface. The diameter of a tungsten electrode was 1.2 mm. Fixed process parameters, which are the results of author's previous study [22], are presented in table 2. Before welding, the grease and residue on the surface of the base metal were removed with acetone; beside the oxidation film was removed with stainless steel brush.

During the experiments, pure argon was employed as a shielding gas flowing from two coaxial nozzles; the flow rate for one was 25 l/min flowing from the laser nozzle and the other one's flow rate was 15 l/min which flew from the TIG nozzle. Coaxial shielding supports the safety of optical elements when operating in an industrial environment. Figure 3 shows the designed fixture and experimental setup. This fixture is capable of changing the D_{LA}, while angel and distance of TIG torch from horizontal are fixed at 35 degrees and 2 mm respectively.

In the present study, the experiments were designed based on a Central Composite Design (CCD) five-level RSM design[19]. Welding speed (1 to 5 mm/s), TIG Current (90 to 130 A) and distance of heat sources (1 to 5 mm) were selected as process independent input variables. Table 3 shows the process input variables and experimental design levels illustrated with coded and actual values, and table 4 shows the designed matrix. Experimental design includes eight experiments as factorial points in cubic vertex, six experiments as axial points and three experiments in the cubic centre as centre point experiments.

In this study, from each welded sample, a specimen was sectioned with respect to the welding direction. The cut specimens were mounted in a phenolic thermosetting resin, conventionally grounded, polished and etched in the Vilella's regent for the dimensional analysis (bicholoric acid 1gr, Hcl 5cc, metyl alcohol 95%). The welding geometry responses (P, W, A), which are shown in figure 1, were measured using Leica MEF 4A optical microscope at a magnification of 50× and were analyzed by a Clemex image analysis software.

4- RESULTS AND DISCUSSION

The weld penetration (P), weld surface width (W), and weld seam area (A) were considered as process responses. An analysis of variance (ANOVA) was conducted in order to investigate "significantly effective parameters" on the laser-TIG hybrid welding process and the interpretation of the results. The results showed that by controlling the laser-TIG input parameters, a proper welding pool could be achieved.

4-1 Weld penetration (P)

A polynomial full quadratic model is used in this analysis. According to the results of an ANOVA run on the weld penetration, table 5, all main parameters are significant. Among quadratic terms, the quadratic term of distance of heat sources, D^2,has a significant effect and other quadratic terms and interactions are insignificant. The ANOVA table of weld penetration indicates that the regression model output fits to the weld penetration with a good estimation. Meanwhile the lack-of fit has been shown to be insignificant. It should be notice that in ANOVA analysis, the best situation occurs when the regression model is significant and Lack-of fit is insignificant at the same time. According to the analysis of results, the final regression yields to eq. 3, this is described in terms of the actual values of the parameters.

$$\mathbf{P\ (\mu m) = 3318.68 - 57.43D + 274.37I - 422.55S - 122.32D^2} \qquad \mathbf{(5)}$$

Figure 4 illustrates the main effect plot of parameters on weld penetration, P. As figure 4 shows by increasing the relative distance of the heat sources, increasing D, weld penetration increases at first, and then it decreases. The reason is that when laser keyhole forms ahead of the arc root in welding direction, D_{LA} is less than D_{ER} in figure 5 and the arc plasma is just above the keyhole. Therefore, the keyhole in the base metal can form only under the arc plasma. Vapor jet from the keyhole goes into and passes through the flexible arc plasma with high speed. Intensive collisions between the particles in vapor jet and arc plasma result in the expansion of the arc plasma. In this case, the electron temperature of arc plasma increases while the electron density decreases. The reason is that the electricity conduction channel in the arc plasma is expanding when such condition occurs. Due to the expansion, the electron density in the spectral acquisition location decreases. Meanwhile, the volume expansion leads to the decrease in collision cross-section of the heavy particles (atoms and ions). As a result, the electron collision probability decreases lead to the increase the electron kinetic energy, which results in the enhancement of the electron temperature[23]. Thus laser inverse Bremsstrahlung absorption coefficient in this case increases which leads to a better energy absorption in the keyhole and increases the weld penetration.

When keyhole forms behind the arc root in welding direction, D_{LA} is higher than D_{ER} in figure 5, therefor influence of laser keyhole on arc plasma is slight. The arc plasma supplies the laser with high temperature welding pool to improve the absorptivity of the laser radiation. Thus the weld penetration increases.

Influence of laser keyhole on arc plasma decreases with the increase in the distance between them. In this situation the laser effects on the solidified weld produced by the TIG welding. Therefore, the laser absorption decreases that result to weld penetration decrease too.

Figure 4 indicates that by increasing the current and decreasing the welding speed, the weld penetration increases. As the welding speed slows down or the current increases, input energy density -the input energy transferred to the material within a unit of distance- ascends and in turn, it leads to an increase in the melted material volume. Thus, the weld penetration is extended.

Figure 6illustrates the variation of weld penetration versus welding speed and current with fixed distance of heat sources at zero level.

As figure 6 shows the point A and it is the only candidate for maximum penetration. This maximum penetration is caused due to the reduction of welding speed and an increase in the current.

Figure 7 illustrates the variation of weld penetration versus distance of heat sources and current with fixed welding speed at zero level.

As figure 7 shows point B has the maximum penetration. This point occurs in the maximum level of current and zero level of distance of heat sources. Figure 4 and the regression equation 3 supports this phenomenon.

Figure 8 shows the residual plot for weld penetration. It is obvious that residues are scattered around the diagonal line and have a normal distribution. This figure approves the early hypothesis, furthermore, the use of F-test and T-test in the analysis are validated. Thus, the final extracted regression model is a proper model for prediction and the investigation of the parameter effects, too.

4-2 Weld surface width (W)

According to the results of an ANOVA run on the weld surface width, table 6, all main parameters are significant. Among interaction terms, the interaction term of distance of heat sources and current, DI, has a significant effect and other interactions while quadratic terms are insignificant.

$$\mathbf{W\ (\mu m) = 5096.74 + 286.38D + 685.06\ I - 656.56\ S + 330.12\ D\times I} \qquad \mathbf{(6)}$$

Figure 9shows the main effect plot of parameters on weld surface width. The effects of the main parameters on weld surface width are the same as the effects of the parameters on the weld penetration. In other words, current and welding speed has direct and reverse effects on the weld surface width, respectively. However, the distance of heat sources has no significant effect on the weld surface width.

Figure 10 illustrates the variation of weld surface width versus welding speed and current with fixed distance of heat sources at zero level.

The results revealed that the reduction of current and an increase in the welding speed, point C in figure 10, reach to an increase in the weld surface width. The reason to this issue is similar to the reason to explanation of figure 4.

Figure 11 illustrates the variation of weld surface width versus distance of heat sourcesand current with fixed welding speed at zero level. The twist of the response surface is caused by the interaction effect of current and distance of heat sources. From figure 11it is crystal clear that increasing the current will lead to an increase in the weld surface width.

4-3 Weld seam area (A)

According to ANOVA results, Table 7, welding speed (S), current (I), and interaction effect of current and distance of heat sources (D×I), are the most significant parameters.

Equation 7 shows the final regression equation of weld seam area in terms of actual values of effective parameters.

$$\mathbf{A\ (mm^2) = 10.14 - 0.38\ D + 1.87\ I - 3.56\ S + 0.66\ S^2 + 0.90\ D \times I} \qquad \mathbf{(7)}$$

In the ANOVA table 7, the distance of heat sources, D, is insignificant. Since the interaction effect of current and distance of heat sources (D×I) is significant, distance of heat sources in the regression model should be considered to develop a hierarchy model.

Figure 12 illustrates the variation of weld seam area versus welding speed and current with fixed distance of heat sources at zero level. The results show that the reduction of current and an increase in the welding speed, point D in figure 12, reach to an increase in the weld seam area. The reason to this issue is similar to the reason that explained for figure 4.

5. OPTIMIZATION

After statistical analysis of data obtained from experimental study and related metallographies, the regression equations 5, 6 and 7 were developed for welding process modeling. These equations explain logical relationships between input variables and responses.

A geometrical dimension of the weld metal is reversely related to mechanical characteristics and joint strength. The research carried out the optimization of laser-TIG hybrid welding process to access optimum welding settings which minimizes geometrical dimensions and makes full penetration. Table 8 offers the criteria for optimization of process parameters.

In table 8, the weight values of all three responses are mentioned and as one may see, weld penetration is more important than the other ones.

The optimization was performed according to criteria mentioned in table 8. Optimum setting was obtained by using Minitab software, which is presented in table 9.

Experiments were carried out under optimum setting in order to validate the optimization results. Metallography of welded samples was performed as mentioned in section 4 and the geometrical dimensions of weld metal were measured by Image Analysis software. Optimum conditions for laser-TIG hybrid welding, real and predicted weld geometrical dimensions and the errors are presented in table 9. Error percentage is considered as the ratio of absolute value of difference to real amount. As shown in table 9, the results validate the optimization results with a good approximation.

To study the mechanical characteristics of the joint in accordance with QW-150 AWS standard in the optimum setting, the weld tensile strength test was performed by using universal tensile test machine made by SCHENCK TREBEL Company. Tensile test samples were prepared by electrical discharge wire cut machine.

Table 10 indicates the results of welding tensile tests. It should be considered that welded samples were fractured of base metal in the optimum setting, figure13. As a result, tensile strength of welded metal is greater than of the base metal. The welding process might have reduced the grain size, produced finer grains in the fusion zone and moderated precipitates which resulted in an increase of tensile strength.

6. CONCLUSIONS:

The following Conclusions can be drawn from the study:

1- Among the process parameters, welding speed is the most effective parameter with a reverse effect on all weld-bead geometrical dimensions; moreover, increase in the TIG current can induce increase of all of geometrical dimensions of weld bead too.
2- Curvatures on the developed response surfaces (3D plots) designate appropriate use of RSM. In addition, it shows that the process parameter ranges have been selected correctly and the optimum setting would exist in the considered parameters space.
3- In this research, by performing optimization process, the following settings can be described as the optimum settings of laser-TIG hybrid welding process: welding speed = 2.5 mm/s, current= 130 A, and distance of heat sources= 2 mm.
4- Under condition of full penetration welding, geometrical dimensions of weld pool has inverse effect on strength of the joint, so that by minimizing geometrical dimensions of weld pool, the tensile strength of welding will be increased.

5- Fracture location in tensile strength test of weldement in optimized setting is on base metal that reveals more strength of the weld metal zone compared to the base metal in finally optimized setting.

References:

1. Ming, G., Z. Xiaoyan, and H. Qianwu, (2007), *Effects of gas shielding parameters on weld penetration of CO2 laser-TIG hybrid welding.* Journal of Materials Processing Technology. **184**(1-3): p. 177-183.

2. Song, G., L. Liu, and P. Wang, (2006), *Overlap welding of magnesium AZ31B sheets using laser-arc hybrid process.* Materials Science and Engineering: A. **429**(1-2): p. 312-319.

3. Liming, L., W. Jifeng, and S. Gang, (2004), *Hybrid laser-TIG welding, laser beam welding and gas tungsten arc welding of AZ31B magnesium alloy.* Materials Science and Engineering A. **381**(1-2): p. 129-133.

4. M. Moradi, M.Ghoreishi., (2010), *Laser welding process optimization using statistical design of experiments, in 18th Annual International Conference on Mechanical Engineering-ISME2010*, Sharif University of Technology, Tehran, Iran.

5. M. Moradi , M.Ghoreishi., (2011), *Influences of laser welding parameters on the geometric profile of NI-base superalloy Rene 80 weld-bead.* Int J Adv Manuf Technol. **55**: p. 205–215.

6. Benyounis K.Y. Olabi A.G. , H.M.S.J., (2008), *Multi-response optimization of CO_2 laser-welding process of austenitic stainless steel.* Optics and Laser Technolog. **40**(1): p. 76-87.

7. Mahmoud Moradi, M.Ghoreishi., Jan Frostevarg, Alexander F.H .Kaplan, (2013), An investigation on stability of laser hybrid arc welding. Opt Laser Eng,. 51, (article in press)

8. Yan, J., M. Gao, and X. Zeng, (2010), *Study on microstructure and mechanical properties of 304 stainless steel joints by TIG, laser and laser-TIG hybrid welding.* Optics and Lasers in Engineering. **48**(4): p. 512-517.

9. Y.Naito, M.M., S.Katayama , *(*2006), *Effect of oxygen in ambient atmosphere on penetration characteristics in single yttrium-aluminum-garnet laser and hybrid welding.* Journal of laser applications. **18**(1): p. 21-27.

10. Zhiyong Li , Wei Wang, Xuyou Wang, Huan Li, (2010), *A study of the radiation of a Nd:YAG laser-MIG hybrid plasma.* Optics & Laser Technology. **42**(1): p. 132-140.

11. Casalino, G., (2007), *Statistical analysis of MIG-laser CO2 hybrid welding of Al-Mg alloy.* Journal of Materials Processing Technology. **191**(1-3): p. 106-110.

12. A.Khorram , M.Ghoreishi., (2011), *CO_2 Laser Welding of a Ti6Al4V Alloy and the Effects of Laser Parameters on the Weld Geometry.* Lasers in engineering. **21**(3-4): p. 135-148.

13. Y. Javid, M.Ghoreishi., S. Shamsaei, (2011), *A Three-Dimensional Heat Transfer Simulation of Laser Full Penetration Welding of Rene-80 Super Alloy.* Lasers in engineering. **22**(1-2): p. 1-11.

14. Tommi Jokinen, M.K., Veli Kujanpaa, *(*2003), *Welding of thick austenitic stainless steel using Nd:YAG laser with filler wire and hybrid process.* Journal of laser applications. **15**(4): p. 220-224.

15. J.S. Kim, T.W., Y. Yoshida,(1995), J. Laser Appl.. **7**(1): p. 38-46.

16. Sujit Ghosal, S.C., (2010), *Estimation and optimization of depth of penetration in hybrid CO2 LASER-MIG welding using ANN-optimization hybrid model.* Int J Adv Manuf Technol. **47**: p. 1149-1157.

17. O.Olsen, C.B.a.F., (2005), *Review of laser hybrid welding.* journal of laser application. **17**(1).

18. R.H. Myers , D.C.M., (1995), *Response surface methodology: Process and product optimization using designed experiments*, New York: Wiley.

19. Montgomery, D.C., (2009), *Design and Analysis of Experiments*, New York: John Wiley.

20. A.I. Khuri, J.A.C., (1996), *Response Surfaces Design and Analysis*, New York: Marcel Dekker.

21. *Derringer, G., and Suich, R.,* (*1980), Simultaneous Optimization of Several Response Variables. Journal of Quality Technology*. ***12***(*4*): p. ***214-219***.

22. M. Moradi, M.Ghoreishi., M.J.Torkamany, J.Sabbaghzadeh, M.J.Hamedi, (2012), *An Investigation on the effect of pulsed Nd:YAG laser welding parameters of stainless steel 1.4418. Advanced Materials Research*. **383-390**: p. *6247-6251*.

23. Liming Liu , M.C., (2011), *Interactions between laser and arc plasma during laser-arc hybrid welding of magnesium alloy*, Optics and Lasers in Engineering. **49**:p. 1224-1231.

Figures:

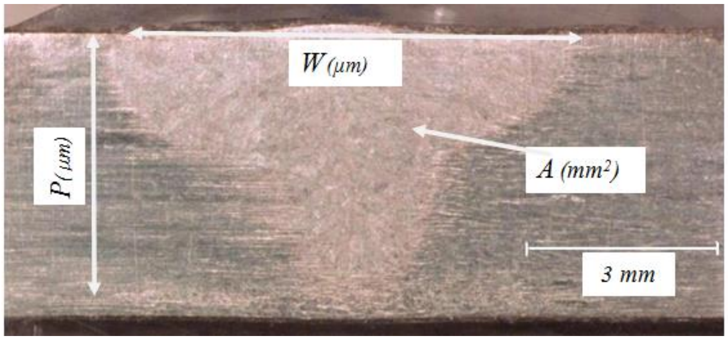

Fig. 1- Specimen cross-section and geometrical responses, typical weld geometry

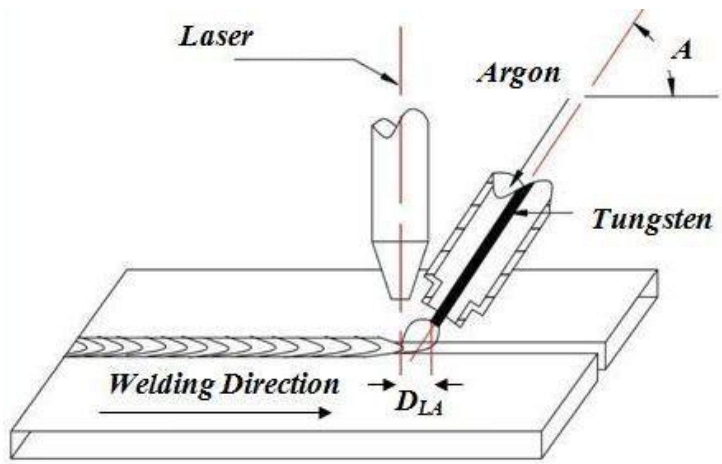

Fig.2- schematic drawing of laser-TIG hybrid welding

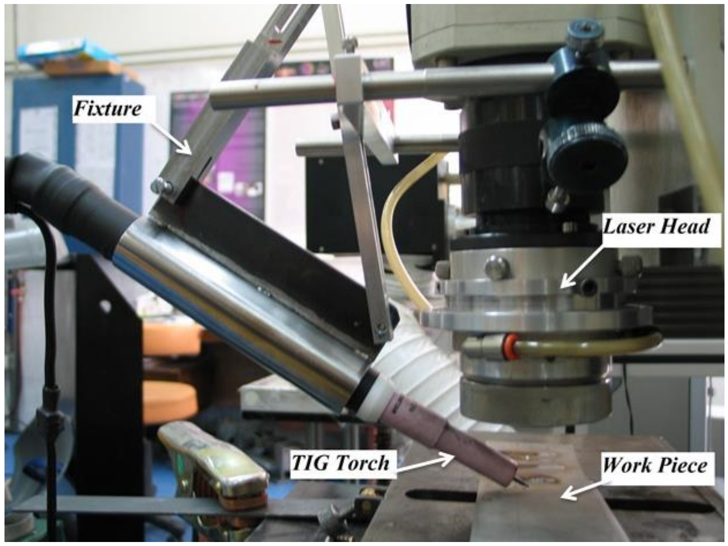

Fig.3 Image of the designed fixture

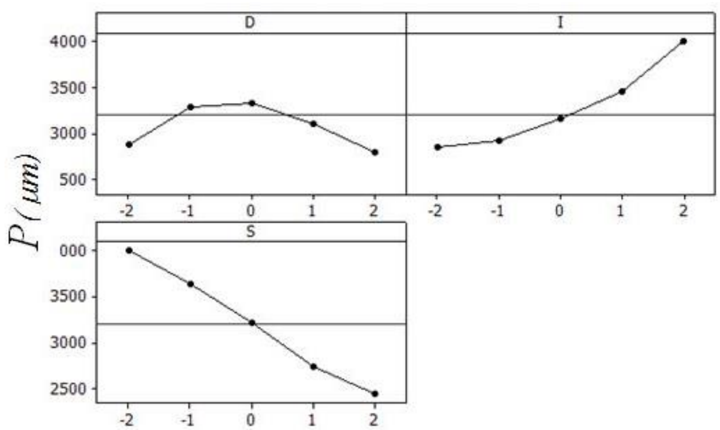

Fig.4 Main effect plot of parameters on weld penetration

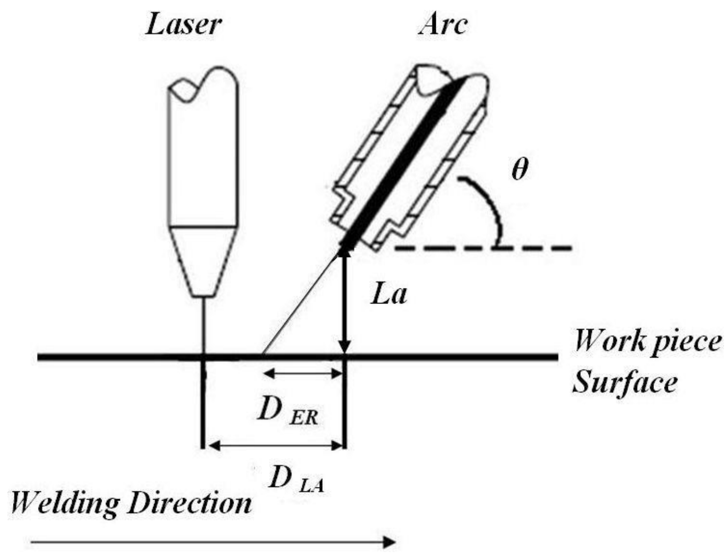

Fig.5 Schematic of the laser and TIG torch distances in the process

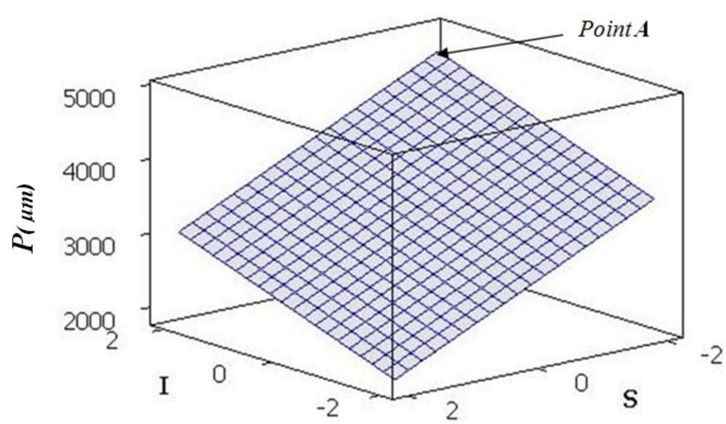

Fig 6. The weld penetration response in terms of the welding speed and current

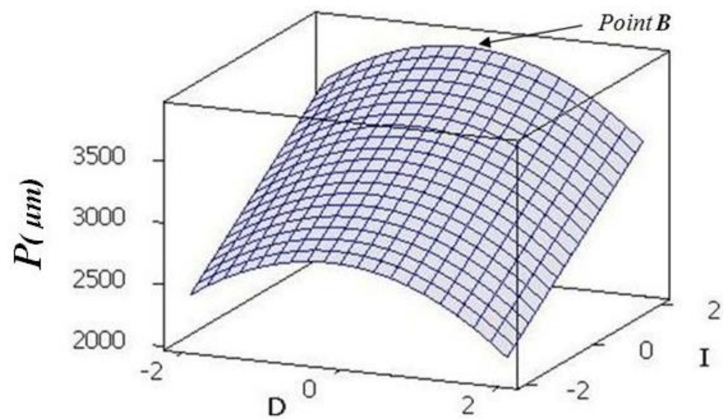

Fig 7. The weld penetration response in terms of the distance of heat sources and current

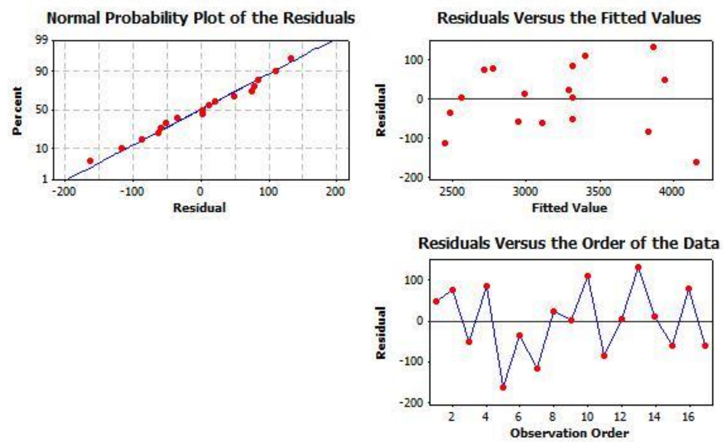

Fig 8. The residual plot for weld penetration

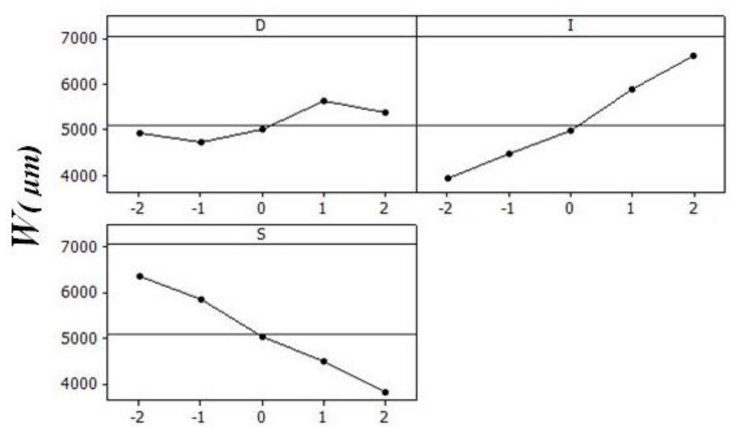

Fig.9 Main effect plot of parameters on weld surface width

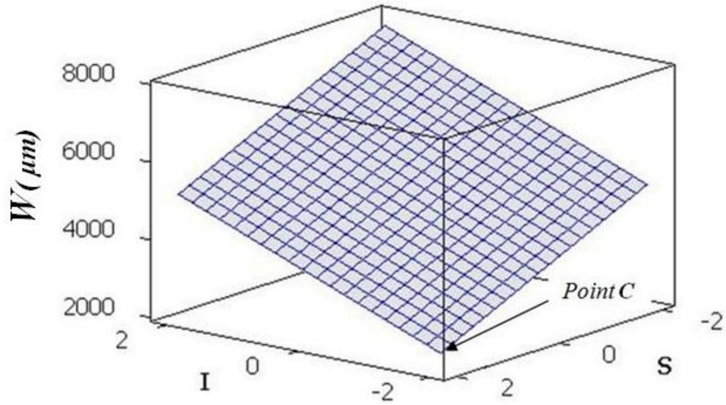

Fig 10. The weld surface width response in terms of the welding speed and current

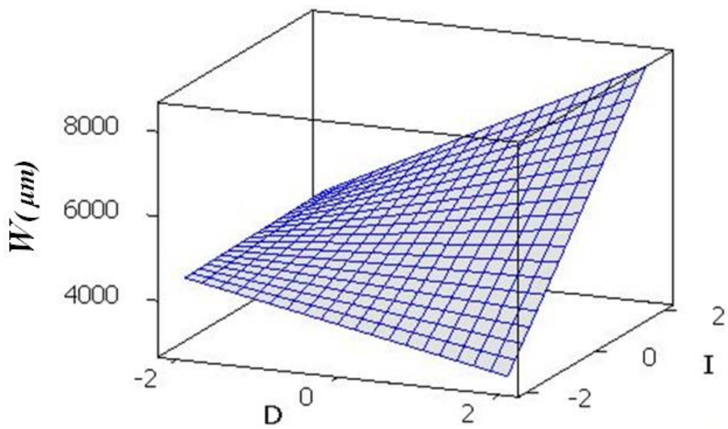

Fig 11. The weld surface width response in terms of the distance of heat sources and current

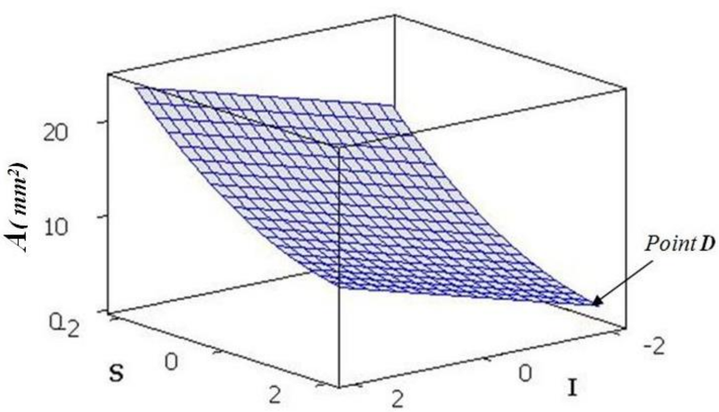

Fig 12. The weld seam area response in terms of the welding speed and current

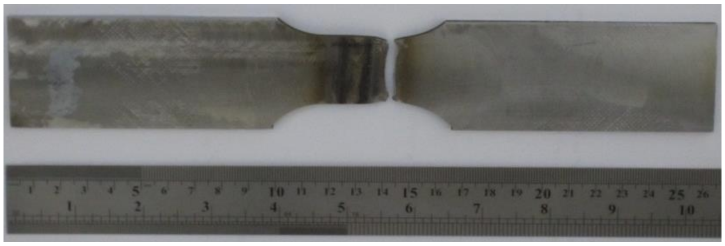

Fig.13. Fractured tensile specimen

Tables:

Table 1. Chemical composition of Stainless steel 1.4418 (wt %)

Fe	Cr	Ni	Mo	Mn	Cu	Si	W	Al	V	C	Co	P	S
Bal	15.91	4.89	0.86	0.72	0.22	0.21	0.15	0.10	0.11	0.037	0.035	0.023	0.005

Table 2- Fixed parameters of experiments

Parameter	Value
Focal plane position	+2 mm
Shielding gas pressure of laser	25 l/min
Shielding gas pressure of TIG	15 l/min
Pulse duration	6 ms
Laser beam frequency	12 Hz
Pulse energy	16.6 J
Torch angle (from the surface)	35º
Wire stickout length	15 mm

Table 3. Independent process parameters and their five values, related to the five design levels (-2 to +2)

Variable	Notation	Unit	-2	-1	0	1	2
D_{LA}	D	[mm]	1	2	3	4	5
Current	I	[A]	90	100	110	120	130
Welding speed	S	[mm/s]	1	2	3	4	5

Table 4. Design matrix, comprising the 17 experiments, expressed by the three input process parameters as design levels

Experiment	Run	D_{LA} [-]	Current [-]	Welding speed [-]
1	14	-1	1	-1
2	1	2	0	0
3	4	0	0	0
4	13	0	0	0
5	7	0	0	-2
6	16	0	0	2
7	12	1	-1	1
8	5	1	-1	-1
9	15	-1	-1	1
10	9	-1	-1	-1
11	8	1	1	-1
12	17	0	0	0

13	3	0	2	0
14	6	1	1	1
15	2	-2	0	0
16	11	0	-2	0
17	10	-1	1	1

Table 5- Modified analyze of variance on weld penetration

Source of variation	Sum of squares	Degree of freedom	Mean squares	*T* value	*F* value	*P* value
Regression	4653491	4	1163373	-	17.60	0.000
D	-111.0	1	-111.0	-1.727	-	0.110
I	228.7	1	228.7	3.559	-	0.004
S	-447.1	1	-447.1	-6.958	-	0.000
D×D	-129.8	1	-129.8	-2.522	-	0.027
Residual Error	793013	12	66084			
Pure Error	9506	2	4753			
Lack-of-Fit	783507	10	78351	-	16.48	0.059
Total	5446504	16				
R-Sq =85.44%	R-Sq (adj)=80.59%					

Table 6- Modified analyze of variance on weld surface width

Source of variation	Sum of squares	Degree of freedom	Mean squares	*T* value	*F* value	*P* value
Regression	16590247	4	4147562	-	31.91	0.000
D	286.4	1	286.4	3.177	-	0.008
I	685.1	1	685.1	7.601	-	0.000
S	-656.6	1	-656.6	7.284	-	0.000
D×I	330.1	1	330.1	2.590	-	0.024
Residual Error	1559750	12	129979			
Pure Error	220369	2	110184			
Lack-of-Fit	1339381	10	133938	-	1.22	0.533
Total	18149996	16				
R-Sq =91.41%	R-Sq (adj)=88.54%					

Table 7- Modified analyze of variance on weld seam area

Source of variation	Sum of squares	Degree of freedom	Mean squares	*T* value	*F* value	*P* value
Regression	279.034	5	55.8067	-	64.74	0.000
D	-0.3830	1	-0.3830	3.177	-	0.127
I	1.8737	1	1.8737	7.601	-	0.000
S	-3.5637	1	-3.5637	-7.284	-	0.000
S×S	0.6600	1	0.6600	3.550	-	0.005
D×I	0.8975	1	0.8975	2.590	-	0.019
Residual Error	9.483	11	0.8621			
Pure Error	2.102	2	1.0508			
Lack-of-Fit	7.381	9	0.8201	-	0.78	0.676
Total	288.516	16				
R-Sq =96.71%	R-Sq (adj) =95.22%					

Table 8. Optimization criteria used in this research

Parameter or	Current	Welding	Distance of	P (μm)	W (μm)	A (mm^2)

Lower limit	90	1	1	2326.13	3430	4.7
Upper limit	130	5	5	4000	7552	20.5
Criterion	Is in	Is in range	Is in range	Max	Min	Min
Weight	-	-	-	5	1	1

Table 9. Validation test result

Exp. No.	I[A]	S[mm/s]	D[mm]	D		P	W	A
1	130	2.5	2	0.8	Actual	3774	5961	13.95
					Predicted	4000	5882.64	14.29
					Error %	5.99	1.31	2.44

Table 10.welding tensile test results

Exp. No.	Yield strength[N/mm^2]	Ultimate strength [N/mm^2]	Elongation [%]	Fracture location
Welded Sample	992.96	1092.14	15	Base metal
Base metal	615	850.5	15	